Programming fracture patterns of thin films

Xiaojie Ma and Yueguang Wei*

Department of Mechanics and Engineering Science, College of Engineering, BIC-ESAT, Peking University, Beijing 100871, China

(Received 7 October 2021; revised 14 December 2021; accepted 25 January 2022; published 14 February 2022)

Controlled fracture presents opportunities for the advanced fabrication of thin films. However, programmability analogous to that of Chinese paper cutting is still challenging, where fracture patterns can be created as required without preformed cracks for guidance. Here, we establish a design framework for tearing adhesive thin films from foldable substrates with such programmability. Our analytical model captures the observed crack behavior, demonstrating that the deflection of crack paths can exceed 90°. Besides, for thick foldable substrates with multiple ridges, we additionally propose a robust method of directional fracture where the cracks are forced to extend along the ridges.

DOI: 10.1103/PhysRevE.105.025002

I. INTRODUCTION

Thin films inserted into engineering systems have been key to modern technologies, which are intended to accomplish a wide range of practical service functions [1], such as thermal [2], tribological [3], optical [4], electrical [5], magnetic [6], and biological [7] functions. Material failure continues to be a technology-limiting barrier, for which fracture is the primary vehicle [1,8,9]. In some circumstances, however, the fracture has desirable consequences, as in pattern formation in controlled fabrication and fragmentation [10–12]. Although the classical fracture theories, which were initially developed by Griffith [13] and Irwin [14], can predict the onset of crack motion well, it is still hard to reliably predict and control the propagation of a crack in general. Recent efforts have analyzed several specific cases where the crack motion was limited in a two-dimensional manifold, presenting a few intrinsic fracture patterns, such as triangle [15], exponential form [16], oscillating [17], spirals [18], and fractal geometries [19]. These intrinsic patterns correspond to specific boundary constraints and load forms with little ability to transform. In contrast, guiding and terminating the paths of cracks can be achieved with the help of preformed cracks [10] or fixed curvature profiles [20]. However, it is challenging to realize the programmability analogous to that of Chinese paper cutting, in which the fracture pattern can be created as required without preformed cracks for guidance.

Here, we overcome this challenge by proposing a method with such programmability. To begin with, we observe the manifold experimental results of tearing adhesive thin films from foldable substrates. According to the observed geometry of origami in the tearing process, we analytically unveil the mechanism of the continuously adjustable tearing angle via an energetic consideration. A design framework is further established based on our analytical solution, quantitatively relating the target patterns to specific substrate configurations and peeling behaviors. Finally, the framework is employed in the case with multiple ridges, additionally showing a robust method of directional fracture.

II. OBSERVATION OF TUNABLE FRACTURE PATTERNS

In common cases, the tearing can be either symmetric or asymmetric. We focus on the cases of symmetric tearing. Additionally, the peeling angle α can range from an acute angle to 180°. When α is too small, local delamination rather than the tearing of thin films occurs (see Appendix B). As a common example, we mainly consider the cases where α is 90°. In addition, the anisotropy has also been reported to distinctly influence the crack motion in thin sheets [21]. Here, however, we aim at the isotropic regime. We use the adhesive biaxially oriented polyimide film whose isotropy is verified in Appendix C. Figures 1(a) and 1(b) show the experimental realization of tearing adhesive thin films from foldable substrates with different substrate configurations, which is defined by the rotation angle β. When β equals 0°, the substrate is an unfolded flat plate. β can reach –90° when the substrate is maximally contracted into a folded state away from the peeling direction. However, because the folded substrate has to provide enough space for the action of peeling thin films, β is unable to reach 90° in the experiment. When β is negative, part of the film adheres to the sides of the substrate for its finite thickness, as shown in Fig. 1(a), but we focus on the part except for the sides of the substrate first. The initially cut rectangular flap is pulled at a constant speed (0.5 mm/s), and then the fracture pattern appears. The setting of the specific β is finished before the initially cut flap further extends. This action ensures that when the cracks propagate, the possible observable compression of the film is avoided. The profile of the thin film torn away from the substrate is equal to the pattern on the substrate due to the congruent mapping (almost no residual in-plane deformation). Figure 1(c) shows four representative results of fracture patterns [α is set to 90° (see Appendices A and D) and β is set to –90°, –45°, 0°, and 45°, respectively], which can be either convergent or divergent.

*weiyg@pku.edu.cn

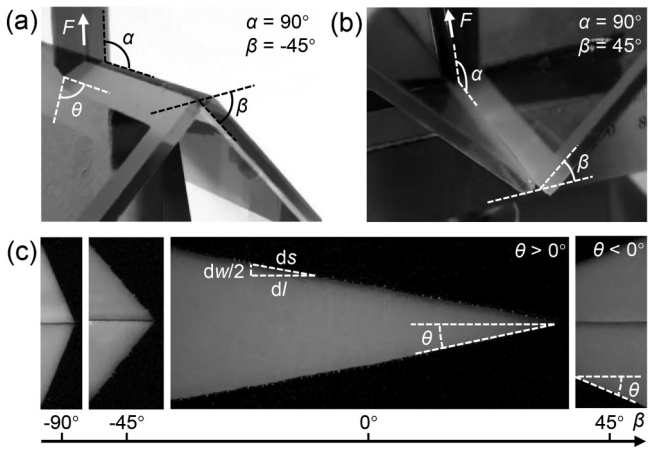

FIG. 1. Experimental realization of tearing action with different substrate configurations [β equals –45 ° in (a) and 45 ° in (b), respectively]. (c) Four representative results of fracture patterns (from left to right, β equals –90 °, –45 °, 0 °, and 45 °, respectively), where the foldable substrate in the case of $\beta = 0°$ is equivalently replaced by a flat substrate. The peeling angle α is set to 90 °, and all initial flaps are made 14 mm wide.

III. THEORY

During the tearing process, the total energy of the system U is considered to be conserved. The work derived from the external force F is translated into the elastic energy of the film U_e for deformation, the fracture work of the film $2Gts$ (G and t are the cleavage energy density and thickness of the film, respectively, and s is the crack path length), and the debonding energy ΓA (Γ is the interfacial energy density between the film and the substrate, and A is the debonding area). When the crack extends an infinitesimal motion,

$$F(1-\cos\alpha)dl = dU_e + 2Gtds + \Gamma dA, \tag{1}$$

where l is the peeling distance along the ridge of the substrate, and $(1-\cos\alpha)dl$ is the distance that F works. Here, the film is considered to be inextensible. The variation of the width between two crack tips dw can be related to ds by the tearing angle θ. However, the relation between dl and ds or dA involves other geometric parameters originating from origami.

To elucidate such geometry, we perform a similar experiment for simulation, folding a piece of paper on a thin dihedral substrate, as shown in Fig. 2. Two geometric features appear immediately: (i) The peeling front is no longer a line segment normal to the ridge of the folded substrate, which is the case of $\beta = 0°$, but a symmetrical polyline with a deflection angle δ. (ii) The actual peeling angle perceived by thin films is a new angle γ rather than α.

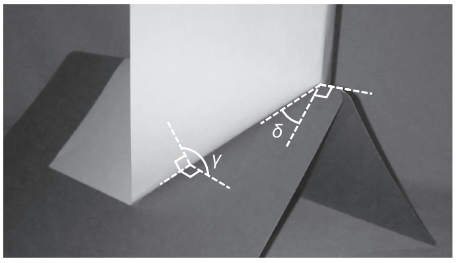

FIG. 2. Illustration of deflection angle δ and local peeling angle γ by folding a piece of paper on a thin dihedral substrate.

In Fig. 2, taking the intersection of the peeling front and the ridge of the substrate (thickness is temporarily ignored here) as origin, the ridge of the substrate as the y axis, and the unit vector along the peeling direction as $(0, \cos\alpha, \sin\alpha)$, we establish the Cartesian coordinates of three-dimensional space. The creases of the folded thin films are at the intersection of the dihedral angle (foldable substrate) and the symmetry plane which can be composed of two noncollinear direction vectors: $(1, 0, 0)$ and $[0, \cos(\alpha/2), \sin(\alpha/2)]$. One vector along one crease can be derived as

$$\vec{r}_i = \left(\cot\beta,\ \cot\frac{\alpha}{2},\ 1\right). \tag{2}$$

One vector on one plane of the substrate normal to the ridge of the substrate is

$$\vec{r}_n = (\cot\beta,\ 0,\ 1). \tag{3}$$

Thus,

$$\cos\delta = \frac{\vec{r}_i \cdot \vec{r}_n}{|\vec{r}_i||\vec{r}_n|}. \tag{4}$$

Then, comprising the sign of δ, we obtain

$$\delta = -\mathrm{sgn}(\beta)\arccos\left(\frac{\sin\frac{\alpha}{2}}{\sqrt{1-\cos^2\frac{\alpha}{2}\cos^2\beta}}\right). \tag{5}$$

To obtain the expression of γ, we analyze planes of thin films divided by the creases. One vector in the plane attached to the substrate is

$$\vec{r}_b = (0,\ -1,\ 0), \tag{6}$$

and the normal vector of such plane is

$$\vec{n}_b = \vec{r}_i \times \vec{r}_b. \tag{7}$$

Similarly, a vector in one plane of the film separated from the substrate is

$$\vec{r}_p = (0,\ \cos\alpha,\ \sin\alpha), \tag{8}$$

and the corresponding normal vector of such plane is

$$\vec{n}_p = \vec{r}_p \times \vec{r}_i. \tag{9}$$

Thus,

$$\cos\gamma = \frac{\vec{n}_b \cdot \vec{n}_p}{|\vec{n}_b||\vec{n}_p|}. \tag{10}$$

Then, we obtain

$$\gamma = \arccos\left(2\cos^2\frac{\alpha}{2}\cos^2\beta - 1\right). \tag{11}$$

While δ is an odd function of β, γ is an even function of β. As for the case that α is set to 90 °, when β increases from

–90 ° to 0 °, δ and γ decrease monotonically from 45 ° to 0 ° and from 180 ° to 90 °, respectively.

Having obtained two geometric parameters originating from origami, we move back to solve Eq. (1). dU_e can be expressed as [22,23]

$$dU_e = \frac{dU_e}{dw} dw, \tag{12}$$

and

$$\frac{dU_e}{d\left(\frac{w}{\cos\delta}\right)} = \frac{U_e}{\frac{w}{\cos\delta}} = 2\sqrt{\frac{(F\cos\delta)B}{\frac{w}{\cos\delta}}}\left(1-\cos\frac{\gamma}{2}\right), \tag{13}$$

where B is the bending stiffness of the film. Namely,

$$\frac{dU_e}{dw} = \frac{U_e}{w} = 2\sqrt{\frac{FB}{w}}\left(1-\cos\frac{\gamma}{2}\right). \tag{14}$$

Additionally,

$$dw = -2\sin\theta ds, \tag{15}$$

$$dA = \left(\frac{w}{\cos\delta}\right)(dl\cos\delta) = wdl, \tag{16}$$

$$dl = \frac{\cos(\delta-\theta)}{\cos\delta} ds. \tag{17}$$

Thus, Eq. (1) becomes

$$F(1-\cos\alpha) = \Gamma w + \left(-2\sin\theta\frac{dU_e}{dw} + 2Gt\right)\frac{\cos\delta}{\cos(\delta-\theta)}. \tag{18}$$

Then,

$$\frac{dF}{d\theta} = 0 \tag{19}$$

leads to

$$\frac{dU_e}{dw}\cos\delta = Gt\sin(\theta-\delta). \tag{20}$$

Inserting Eq. (20) in Eq. (18) yields

$$F(1-\cos\alpha) = \Gamma w + 2Gt\frac{-\sin\theta\sin(\theta-\delta)+\cos\delta}{\cos(\delta-\theta)}. \tag{21}$$

Taking two approximations into consideration [(i) $\Gamma w \gg Gt$ in the initial tearing process, and (ii) $\zeta \triangleq [-\sin\theta\sin(\theta-\delta)+\cos\delta]/\cos(\delta-\theta) \lesssim 1$ (see Appendix E)], we obtain

$$F = \frac{\Gamma w}{1-\cos\alpha}. \tag{22}$$

The combination of Eqs. (14), (20), and (22) leads to

$$\sin(\theta-\delta) = \frac{\sqrt{2\Gamma B}}{Gt}\tan\frac{\gamma}{4}. \tag{23}$$

We introduce

$$\theta_0 \triangleq \theta|_{\alpha=180^\circ,\beta=0^\circ}, \tag{24}$$

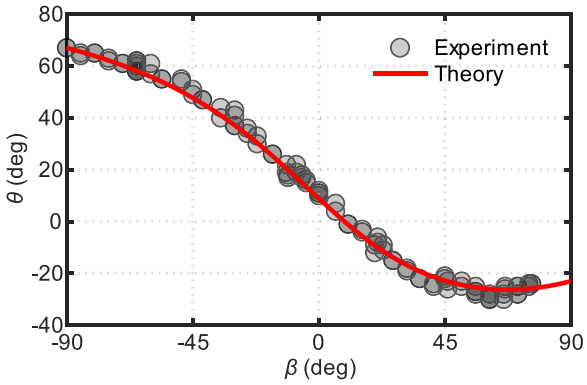

FIG. 3. Tearing angle θ predicted by our analytical solution (solid curve) and measured by our experiments (markers).

and can express Eq. (23) as

$$\theta = \arcsin\left(\sin\theta_0\tan\frac{\gamma}{4}\right) + \delta. \tag{25}$$

θ_0 satisfies

$$\sin\theta_0 = \frac{\sqrt{2\Gamma B}}{Gt}, \tag{26}$$

which comprises all properties of material and interface that can affect the tearing angle but excludes the effect from the possible plastic deformation of the film [15,22]. In our experiments shown in Fig. 1, θ_0 is 22 ° (see Appendix C). Figure 3 demonstrates that our analytical solution captures the evolution of experimental tearing behavior almost perfectly. The variation range of θ exceeds 90 °. When β is –90 °, θ reaches its maximum 67 °. When β is between 45 ° and 90 °, θ can reach its theoretical minimum, which is about –26 °.

Furthermore, according to our solution, when α equals 90 °, the cases of $\forall\theta_0 \in (0^\circ, 90^\circ)$ share some features: (i) The theoretical maximum of tearing angle always appears at $\beta = -90^\circ$ [Fig. 4(a)]. (ii) The theoretical minimum of tearing angle always appears at $\beta \in (45^\circ, 90^\circ)$ [Fig. 4(a)]. (iii) The theoretical variation range of θ steadily exceeds 90 ° [Fig. 4(b)].

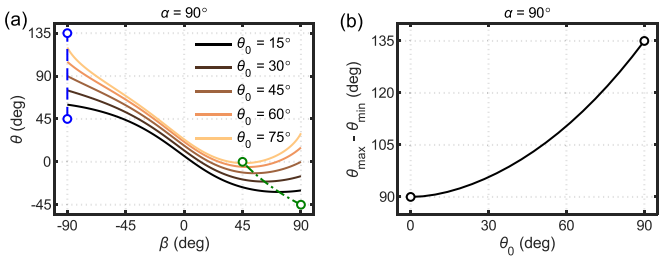

FIG. 4. (a) The theoretical solution of tearing angle θ for five different representative θ_0, where the maximum of tearing angle always appears at $\beta = -90^\circ$ and the minimum of tearing angle always appears at $\beta \in (45^\circ, 90^\circ)$. In (a), the theoretical maximum of tearing angle for $\theta_0 \in (0^\circ, 90^\circ)$ is illustrated by the dashed line and the theoretical minimum of tearing angle for $\theta_0 \in (0^\circ, 90^\circ)$ is illustrated by the dash-dot curve. (b) The theoretical variation range of θ for $\theta_0 \in (0^\circ, 90^\circ)$, which is steadily larger than 90 °. In [(a),(b)], the peeling angle α is set to 90 °.

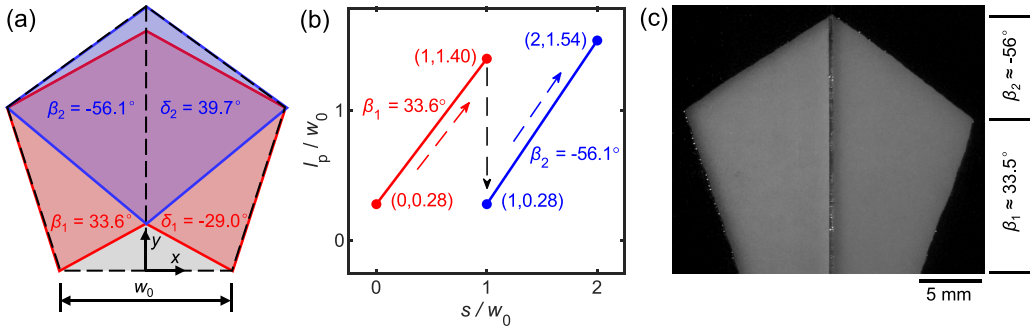

FIG. 5. The process of programming a regular pentagonal target fracture pattern. (a) The geometric analysis of the target pattern with initial width w_0, which provides the selected dihedral angle β and corresponding deflection angle δ from our analytical solution. (b) The mapping relation between the peeling distance l_p and the length of the crack path s in two stages. (c) The experimental realization of the target fracture pattern.

Finally, we discuss the case of $\beta < 0$, in which part of the film adheres to the sides (groove) of the foldable substrate for its finite thickness [Fig. 1(a)]. We can divide the total external force F into two parts, F_{out} and F_{in}. F_{in} is applied to peel the film from the groove, while F_{out} is used to tear the film outside the groove. Therefore, in previous equations where the thickness of the substrate is ignored, F is equivalent to F_{out} here for negative β, which does not change our analytical solution Eq. (25), emphasizing the local character of tearing behavior.

IV. PROGRAMMING FRACTURE PATTERNS OF THIN FILMS

In experiments described before, β is fixed, and two symmetric boundaries of fracture pattern are straight. Actually, β can be freely adjusted in the tearing process. Adjusting β when the tearing is stopped, we can not only realize the slightly kinked cracks [24], but also produce the cracks with large kink angles. On the other hand, the crack paths become curves when β is adjusted continuously during the process (see Appendix F and the movie in the Supplemental Material [25]). These tunable crack paths make programming fracture patterns of thin films feasible.

To illustrate the basic steps of such programming, we take the target pattern as a regular pentagon as an example. As shown in Fig. 5(a), two stages connected by a kink are needed to complete the target pattern. We first select the corresponding β and δ from our analytical solution, which are denoted by (β_1, δ_1) and (β_2, δ_2), respectively. Then, we precisely calculate different peeling distances for two stages to ensure equal crack length at each stage. In such calculations, the deflection angle δ plays an important role. Along the direction defined by δ, the length of the crack path can be mapped to the path along the ridge of the substrate, as shown by two shadows (red and blue) in Fig. 5(a). For the cases we focus on (α is set to 90 °), at each stage the increase of the peeling distance l_p equals the change of l. According to Eq. (17), the relation between l_p and s in two stages can be calculated and is illustrated in Fig. 5(b). Finally, under the calculated guidance, we successfully realize the target fracture pattern [Fig. 5(c)]. Following these basic steps, one can readily program other fracture patterns according to our analytical solution, including the curving patterns, by continuously altering β during the tearing process.

Because of the inevitable experimental error, it is still challenging to precisely realize the directional fracture such as the parallel crack paths (θ equals 0 °). In contrast, the divergence of the fracture pattern for $\beta = 45°$ and the convergence of the fracture pattern for $\beta \leqslant 0°$ are robust. These two robust regimes imply another method of directional fracture. As for cases with two ridges, the geometric parameter β thereupon changes when the cracks extend across the ridges. A specific example is that when cracks extend near the ridge of the thick

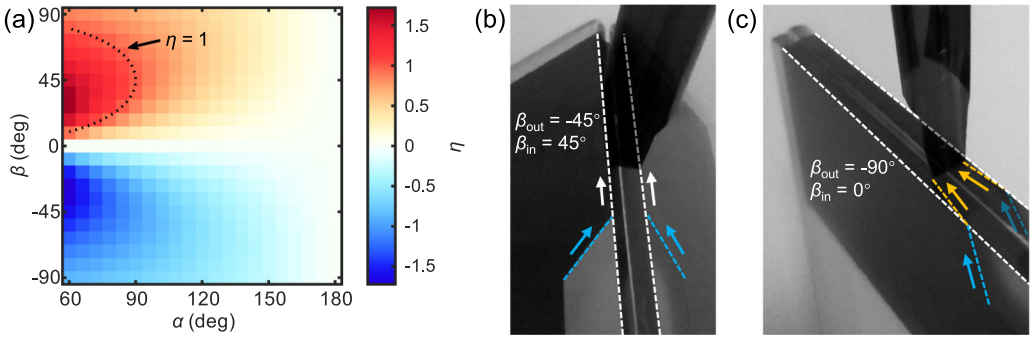

FIG. 6. (a) Mapping of η for α ranging from 60 ° to 180 ° and β ranging from –90 ° to 90 °, on which the curve of $\eta = 1$ (dotted curve) is also plotted. Experimental realization of directional fracture along the ridges (b) and kinking crack paths across ridges (c) for thick foldable substrates. (β_{out}, β_{in}) equals (–45 °, 45 °) in (b) and (–90 °, 0 °) in (c). The thickness of the substrate is 3 mm.

foldable substrate, a groove bordered by two actual ridges appears [Fig. 1(a)], which is secondary in the above analyses where we mainly focus on the fracture outside such groove. If β outside (β_{out}) and inside (β_{in}) the groove correspond to the convergent and divergent fracture patterns, respectively, the cracks will be forced to extend along the ridges. To quantify the condition of such a phenomenon, we introduce a geometric parameter:

$$\eta \triangleq -\frac{\sin\delta}{\tan\frac{\gamma}{4}}. \tag{27}$$

Thus, the divergent phenomenon of fracture pattern is equivalent to $\eta > \sin\theta_0$. The mapping of η for α ranging from 60° to 180° and β ranging from -90° to 90° is presented in Fig. 6(a). When α is less than 90°, η can be larger than 1 [the left side of the dotted curve in Fig. 6(a)], definitely resulting in a divergent fracture pattern. In particular, when α equals 90° and β equals 45°, η equals 1. Across the ridges of thick foldable substrates, the jump value of β is 90°. We thus propose a method of directional fracture: setting β outside the groove to -45°. As a result, we obtain a robust parallel fracture pattern along the ridges, as shown in Fig. 6(b). In addition, a common phenomenon of kinking crack paths across the ridges is illustrated in Fig. 6(c).

V. CONCLUSION

In conclusion, we have demonstrated a strategy of programming fracture patterns of thin films on demand without preformed cracks for guidance. We anticipate that our design framework can be extended in various directions. First, asymmetric tearing would lead to a universal design regime, sharing the same geometric mechanism with the symmetric tearing we have discussed. Second, various origami structures [26,27], whose building block is just the simple dihedral angle that we have taken as the configuration of the foldable substrate, could undoubtedly enrich the possible target patterns. Third, our design framework might provide an alternative perspective to understand the fracture pattern on curved surfaces [16,28] by taking the resulting fracture patterns as the target patterns to consider the instantaneous tearing mechanism inversely. Finally, except for one angle parameter θ_0 comprising all properties of material and interface that can affect the tearing angle, all parameters in our analytical solution, Eq. (25), are purely geometric. Therefore, our results can readily be generalized to other similar film-substrate systems across materials and scales, leading to potential applications such as facilitating the development of artificial nanostructures [29,30]. However, when the torn thin film is multilayer [29], the geometry-dependent bending stiffness may require additional consideration [31–33].

ACKNOWLEDGMENTS

We thank Jingru Song and Xiaoming Liu for their technical support. X.M. thanks Pascal Damman, Hao Long, and Bin Li for helpful discussions; Hanbin Yin, Min Ru, Shiyuan Shao, and Fanyang Mo for useful suggestions on experiments; and Ziwei Liu for technical assistance. This work was supported by the National Natural Science Foundation of China through Grants No. 11890681, No. 12032001, and No. 11521202.

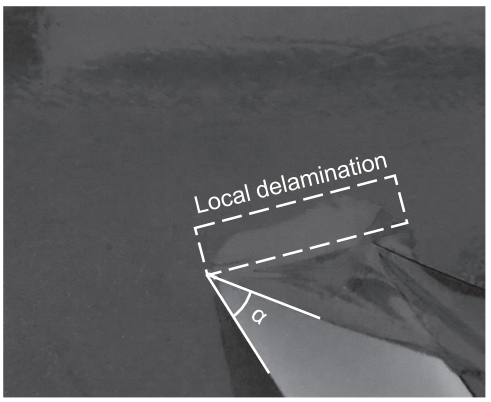

FIG. 7. The occurrence of local delamination rather than tearing for a small acute peeling angle.

APPENDIX A: MATERIAL PREPARATION AND EXPERIMENTAL MEASUREMENT

We used a strip of wide transparent tape to connect two plates, obtaining the foldable substrate. These plates could be thick (thickness: 3 mm) or thin (thickness: 0.65 mm). Except for the simulation experiment of origami (Fig. 2) and the tearing experiment with curved crack paths (see Appendix F and the movie in the Supplemental Material [25]), where the thin plates were used as the substrates, the substrates used in all tearing experiments were made by thick plates. The thick plates we used were 3 mm thick frosted glass plates, while the thin plates were plastic with 0.65 mm thickness. Additionally, except for the tearing experiment shown in Appendix C where a piece of adhesive monoaxially oriented polyimide film (purchased from Runsea company) was used, the torn films used in all experiments were adhesive biaxially oriented polyimide films (purchased from Runsea company). The paper used in Fig. 2 was a piece of A4 paper. The initial flaps, which were

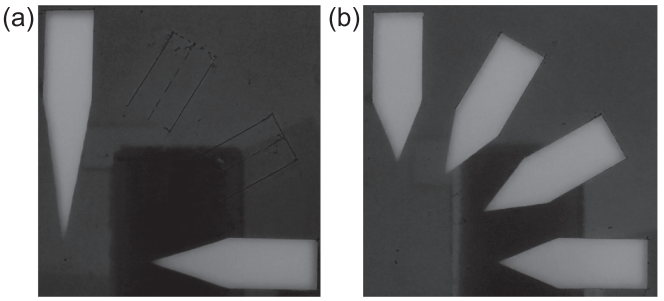

FIG. 8. (a) Significantly different tearing angles for two initially cut flaps with different orientations in a piece of adhesive monoaxially oriented polyimide film, which implies the evident anisotropy of the film. (b) The same tearing angle for four initially cut flaps with different orientations in a piece of adhesive biaxially oriented polyimide film that we mention in the main text, which demonstrates the isotropy of the film. The used substrates are flat ($\beta = 0^\circ$). The peeling angle α is set to 180°, and all initial flaps are made 14 mm wide. In (b), θ_0 is measured to be 22°.

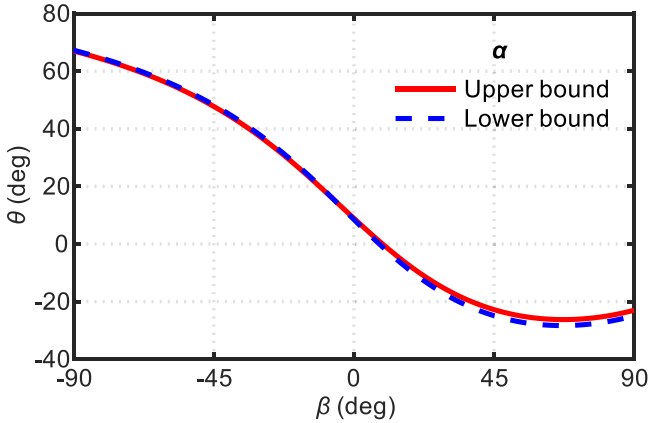

FIG. 9. Theoretical estimation of the effect of the slight change of peeling angle α on the tearing angle θ, where two boundary values of α are illustrated in Eq. (D2), and θ_0 is taken as 22°.

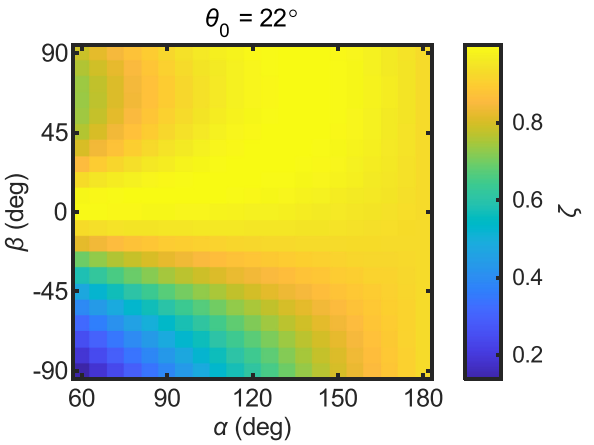

FIG. 11. The mapping of ζ for α ranging from 60° to 180° and β ranging from –90° to 90°, where θ_0 is taken as 22°, and we use our analytical solution [Eqs. (5), (11), and (25)]. This mapping shows that $\zeta < 1$. Given the slight difference between the theoretical prediction and experimental results, as shown in Fig. 3, we choose $\zeta \lesssim 1$ as the second approximation.

peeled from the substrates before the tearing action, were cut by a knife. We additionally used a transparent tape (3M-600) to connect the initial flap and the clamp of the testing machine (Instron 5942). The length of this transparent tape was ensured more than 300 mm, which was much larger than the typical scale of flap torn from the substrate, ensuring the almost fixed peeling angle during the tearing process, whose detailed analysis is shown in Appendix D. All photos and a movie in the Supplemental Material [25] were shown in black-and-white mode, whose gray-scale values were set to the blue values (in RGB color mode) of the original corresponding photos and movie except for Fig. 2 where the red values were used.

APPENDIX B: OCCURRENCE OF LOCAL DELAMINATION FOR SMALL PEELING ANGLE

When the initial flap was peeled with a small acute peeling angle, local delamination rather than tearing happened, as shown in Fig. 7.

APPENDIX C: EVIDENCE OF ISOTROPY

The isotropy of the adhesive biaxially oriented polyimide film we used was verified in Fig. 8. Meanwhile, θ_0 could be measured to be 22°.

APPENDIX D: ANALYSIS OF THE SLIGHTLY DEVIATED PEELING ANGLE

In our tearing experiments, the length of the connection tape between the initial flap and the clamp of the testing machine was finite but was ensured to be more than 300 mm, which was expected to ensure the change of the peeling angle α during the tearing process was tiny.

From the experimental point of view, the fact that the boundary of the fracture pattern for specific β is straight rather than evidently curved [Fig. 1(c)] implies that the effect of the slightly deviated peeling angle on the tearing angle is marginal.

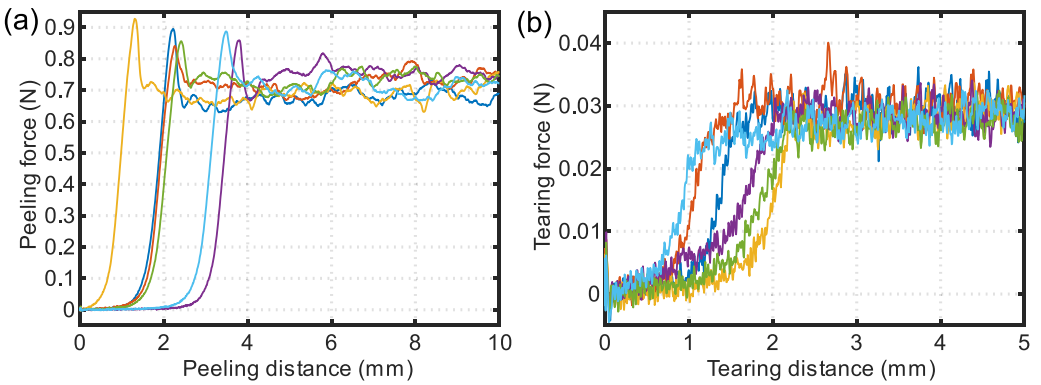

FIG. 10. (a) The peeling force in the peeling test [22] (the peeling angle is 90° and the width of the adhesive flap w_0 was 14 mm), which shows that Γw_0 is about 0.7 N (six repeated experiments). (b) The tearing force in the trouser test [22], which shows that $Gt/2$ is about 0.03 N (six repeated experiments). Thus, $(Gt)/(\Gamma w_0) \approx 9\%$. The used films in [(a),(b)] are the adhesive biaxially oriented polyimide films, and the used substrates in (a) are the thick substrate, same as the tearing experiments.

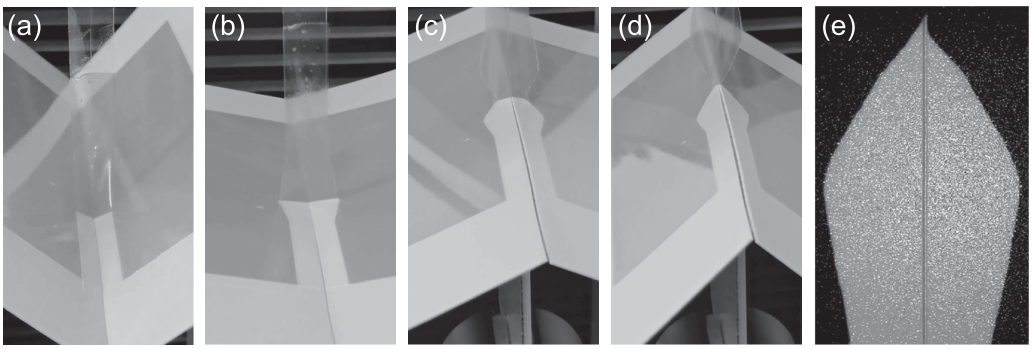

FIG. 12. [(a)–(d)] The process of tearing adhesive thin film by continuously adjusting β from a positive value to a negative value, which is shown by the snapshots of the movie in the Supplemental Material [25]. (e) The resulting fracture pattern with curved crack paths. The initial flap is made 14 mm wide, and is pulled at a constant speed (2 mm/s). We note that β is simply adjusted by hand in this case, which leads to the slight asymmetry of the resulting fracture pattern.

In addition, we can also theoretically estimate the effect of the variation of peeling angle α on the tearing angle θ. As for the convergent fracture pattern, when α and β are both fixed and the width of the initial flap is 14 mm, the total l_p is expected to be $7\cot\theta$ mm. However, when the cracks extend parallel or divergent, the total l_p does not exist. In Figs. 1 and 3, except for the case that $\alpha = 90^\circ$ and $\beta = 0^\circ$ shown in Fig. 1(c), the maximum peeling distance of the testing machine could be set to 20 mm, and the theoretical l_p becomes

$$l_p = \begin{cases} \min\{7\cot\theta \text{ mm}, 20 \text{ mm}\}, & \beta < 0^\circ \\ 20 \text{ mm}, & \beta > 0^\circ \end{cases}. \tag{D1}$$

Thus, when the initial peeling angle is set as 90°,

$$90^\circ - \tan\left(\frac{l_p}{300 \text{ mm}}\right) < \alpha \leqslant 90^\circ. \tag{D2}$$

We simply use these two boundary values of α to estimate the effect of the slight change of peeling angle α on the tearing angle θ in Fig. 9, demonstrating that such effect is expected to be marginal.

APPENDIX E: TWO APPROXIMATIONS

In Sec. III, we used two approximations to obtain Eq. (22): (i) $\Gamma w \gg Gt$ in the initial tearing process, and (ii) $\zeta \lesssim 1$; these are illustrated in Figs. 10 and 11, respectively.

APPENDIX F: A CASE OF CURVED CRACK PATHS

One can readily produce a pair of curved crack paths by tearing with continuously adjusted β. Here, Fig. 12 presents a simple case. We note that when β increases continuously, β should be adjusted relatively slowly (compared to the pulling speed) to avoid the film near the substrate under observable compression, which may affect the precision of the obtained fracture pattern.

[1] L. B. Freund and S. Suresh, *Thin Film Materials: Stress, Defect Formation and Surface Evolution* (Cambridge University Press, Cambridge, 2004).
[2] N. P. Padture, M. Gell, and E. H. Jordan, Thermal barrier coatings for gas-turbine engine applications, Science **296**, 280 (2002).
[3] A. Leyland and A. Matthews, On the significance of the H/E ratio in wear control: A nanocomposite coating approach to optimised tribological behaviour, Wear **246**, 1 (2000).
[4] F. Bonaccorso, Z. Sun, T. Hasan, and A. C. Ferrari, Graphene photonics and optoelectronics, Nat. Photonics **4**, 611 (2010).
[5] J. A. Rogers, T. Someya, and Y. Huang, Materials and mechanics for stretchable electronics, Science **327**, 1603 (2010).
[6] J. Wang, J. B. Neaton, H. Zheng, V. Nagarajan, S. B. Ogale, B. Liu, D. Viehland, V. Vaithyanathan, D. G. Schlom, U. V. Waghmare *et al.*, Epitaxial BiFeO3 multiferroic thin film heterostructures, Science **299**, 1719 (2003).
[7] H. Yuk, C. E. Varela, C. S. Nabzdyk, X. Mao, R. F. Padera, E. T. Roche, and X. Zhao, Dry double-sided tape for adhesion of wet tissues and devices, Nature (London) **575**, 169 (2019).
[8] A. Livne, E. Bouchbinder, I. Svetlizky, and J. Fineberg, The near-tip fields of fast cracks, Science **327**, 1359 (2010).
[9] J. W. Hutchinson and Z. Suo, Mixed-mode cracking in layered materials, Adv. Appl. Mech. **29**, 63 (1991).
[10] K. H. Nam, I. H. Park, and S. H. Ko, Patterning by controlled cracking, Nature (London) **485**, 221 (2012).
[11] M. Chen, Z. Wang, X. Ge, Z. Wang, K. Fujisawa, J. Xia, Q. Zeng, K. Li, T. Zhang, Q. Zhang *et al.*, Controlled fragmentation of single-atom-thick polycrystalline graphene, Matter **2**, 666 (2020).
[12] B. Ni and H. Gao, Harness the power of fracture: Controlled fragmentation of graphene via substrate necking, Matter **2**, 521 (2020).
[13] A. A. Griffith, The phenomena of rupture and flow in solids, Philos. Trans. R. Soc., A **221**, 163 (1921).
[14] G. R. Irwin, Analysis of stresses and strains near the end of a crack traversing a plate, J. Appl. Mech. **24**, 361 (1957).
[15] E. Hamm, P. Reis, M. LeBlanc, B. Roman, and E. Cerda, Tearing as a test for mechanical characterization of thin adhesive films, Nat. Mater. **7**, 386 (2008).

[16] O. Kruglova, F. Brau, D. Villers, and P. Damman, How Geometry Controls the Tearing of Adhesive Thin Films on Curved Surfaces, Phys. Rev. Lett. **107**, 164303 (2011).
[17] R. D. Deegan, P. J. Petersan, M. Marder, and H. L. Swinney, Oscillating Fracture Paths in Rubber, Phys. Rev. Lett. **88**, 014304 (2001).
[18] K. T. Leung, L. Józsa, M. Ravasz, and Z. Néda, Spiral cracks without twisting, Nature (London) **410**, 166 (2001).
[19] A. T. Skjeltorp and P. Meakin, Fracture in microsphere monolayers studied by experiment and computer simulation, Nature (London) **335**, 424 (1988).
[20] N. P. Mitchell, V. Koning, V. Vitelli, and W. T. Irvine, Fracture in sheets draped on curved surfaces, Nat. Mater. **16**, 89 (2017).
[21] A. Takei, B. Roman, J. Bico, E. Hamm, and F. Melo, Forbidden Directions for the Fracture of Thin Anisotropic Sheets: An Analogy with the Wulff Plot, Phys. Rev. Lett. **110**, 144301 (2013).
[22] B. Roman, Fracture path in brittle thin sheets: A unifying review on tearing, Int. J. Fract. **182**, 209 (2013).
[23] E. Gao, S.-Z. Lin, Z. Qin, M. J. Buehler, X.-Q. Feng, and Z. Xu, Mechanical exfoliation of two-dimensional materials, J. Mech. Phys. Solids **115**, 248 (2018).
[24] B. Cotterell and J. R. Rice, Slightly curved or kinked cracks, Int. J. Fract. **16**, 155 (1980).
[25] See Supplemental Material at http://link.aps.org/supplemental/10.1103/PhysRevE.105.025002 for a movie of the production of a pair of curved crack paths.
[26] Y. Chen, R. Peng, and Z. You, Origami of thick panels, Science **349**, 396 (2015).
[27] J. A. Faber, F. Arrieta, and A. R. Studart, Bioinspired spring origami, Science **359**, 1386 (2018).
[28] B. Li, D. Millán, A. Torres-Sánchez, B. Roman, and M. Arroyo, A variational model of fracture for tearing brittle thin sheets, J. Mech. Phys. Solids **119**, 334 (2018).
[29] J. Annett and G. L. Cross, Self-assembly of graphene ribbons by spontaneous self-tearing and peeling from a substrate, Nature (London) **535**, 271 (2016).
[30] H. Chen, X. Zhang, Y. Zhang, D. Wang, D. Bao, Y. Que, W. Xiao, S. Du, M. Ouyang, S. T. Pantelides *et al.*, Atomically precise, custom-design origami graphene nanostructures, Science **365**, 1036 (2019).
[31] F. Pan, G. Wang, L. Liu, Y. Chen, Z. Zhang, and X. Shi, Bending induced interlayer shearing, rippling and kink buckling of multilayered graphene sheets, J. Mech. Phys. Solids **122**, 340 (2019).
[32] E. Han, J. Yu, E. Annevelink, J. Son, D. A. Kang, K. Watanabe, T. Taniguchi, E. Ertekin, P. Y. Huang, and A. M. van der Zande, Ultrasoft slip-mediated bending in few-layer graphene, Nat. Mater. **19**, 305 (2019).
[33] X. Ma, L. Liu, Z. Zhang, and Y. Wei, A method to determine the geometry-dependent bending stiffness of multilayer graphene sheets, J. Appl. Mech. **88**, 011004 (2021).